catalysts

MDPI

Article

Curcumin Doped SiO_2/TiO_2 Nanocomposites for Enhanced Photocatalytic Reduction of Cr (VI) under Visible Light

Zhiying Yan [1,*], Zijuan He [1], Mi Li [1], Lin Zhang [1], Yao Luo [1], Jiao He [1], Yongjuan Chen [1] and Jiaqiang Wang [2,*]

1 School of Chemical Sciences & Technology, Yunnan University, Kunming 650091, China; zijuanhe@outlook.com (Z.H.); Lm8827@outlook.com (M.L.); echo928534098@mail.ynu.edu.cn (L.Z.); yaoluo1982@outlook.com (Y.L.); hejiao@ynu.edu.cn (J.H.); yongjuanchen@ynu.edu.cn (Y.C.)

2 National Center for International Research on Photoelectric and Energy Materials, Yunnan Provincial Collaborative Innovation Center of Green Chemistry for Lignite Energy, Yunnan Province Engineering Research Center of Photocatalytic Treatment of Industrial Wastewater, The Universities' Center for Photocatalytic Treatment of Pollutants in Yunnan Province, Kunming 650091, China

* Correspondence: zhyyan@ynu.edu.cn (Z.Y.); jqwang@ynu.edu.cn (J.W.); Tel.: +86-871-6503-1567 (Z.Y. & J.W.)

Received: 20 July 2020; Accepted: 14 August 2020; Published: 17 August 2020

Abstract: In order to further improve the photocatalytic performance of the SiO_2/TiO_2 composite under visible light irradiation, curcumin-doped SiO_2/TiO_2 nanocomposites were synthesized via directly incorporating it into the structure of SiO_2/TiO_2 during the synthesis using an inexpensive and readily available natural pigment (curcumin) as doping agent. The physicochemical properties of SiO_2/TiO_2 nanocomposites were characterized in detail by X-ray diffraction, transmission electron microscopy, Fourier transform-infrared spectroscopy, N_2 adsorption–desorption isotherms, X-ray photoelectron spectroscopy, and UV-vis diffuse reflectance spectroscopy. The results indicate that all SiO_2/TiO_2 nanocomposites exhibited an anatase phase with a typical mesoporous structure. It was found that the dope of curcumin in the SiO_2/TiO_2 composite could decrease the crystal size, slightly improve the specific surface areas, significantly enhance the visible light absorption, and effectively narrow the band gap energy from 3.04 to 10(eV). Compared with bare SiO_2/TiO_2, the curcumin-doped SiO_2/TiO_2 resulted in enhanced photocatalytic reduction activity for Cr(VI) under visible light irradiation, and the CTS (12) sample with the appropriate content of curcumin of 12 wt % shows the photocatalytic yield reaching 100% within 2.5 hours, which is larger than CT (12) without silica. This could be attributed to the curcumin doping and the synergetic effects of SiO_2 and TiO_2 in SiO_2/TiO_2 nanocomposites.

Keywords: curcumin pigment; SiO_2/TiO_2 nanocomposites; visible photocatalyst; reduction of Cr (VI)

1. Introduction

Titanium dioxide photocatalysis is considered as a promising and effective technology for the removal of organic pollutants from aquatic systems due to its non-toxic, low cost, and resistance to photochemical and chemical corrosion [1,2]. Anatase, rutile, and brookite are three polymorphs of TiO_2, among which anatase is the most active one in the photocatalytic process [3]. In order to improve its photocatalytic activity, novel TiO_2-based photocatalysts were designed and synthesized through both the structural modification and the compositional change [3,4]. Compared to pure titanium oxide, SiO_2/TiO_2 composite is found to be more conducive to improve the photocatalytic activity and the separation of products after the reaction [5–8]. For examples, Hou et al. [9] found that the dope of SiO_2 significantly changed the phase composition, specific surface area, microstructure,

and the photocatalytic activity of TiO_2. Mahyar et al. [10] reported that the specific surface area of a catalyst increased by doping the SiO_2, which allowed an increase in adsorption of pollutant molecules, thus, improving photocatalytic activity of TiO_2. Meng et al. [11] reported that the increase of the photocatalytic activity resulted from the addition of silica, which reduced the particle size, improved the specific surface area and thermal stability of anatase. However, like TiO_2, SiO_2/TiO_2 composites can only be excited under the UV light since the band gap energy of TiO_2 is 3.2 eV. Therefore, there is a growing interest in doping modification of SiO_2/TiO_2 for improving its visible light photocatalytic performance. For examples, Ghanbari et al. [12] found that doping N and F in TiO_2/SiO_2 nanoparticles led to the fully anatase crystalline structure, the minimized agglomeration of synthesized nanoparticles, and enhanced photocatalytic activity under solar and visible light irradiation. Liu et al. [13] prepared F/W co-doped TiO_2-SiO_2 composite aerogels with the higher photoelectron conversion efficiency, which are advantageous to degrade the pollutant RhB in the aqueous solution under visible light irradiation.

Beside element doping, the dye sensitization is also proved to be an effective method to increase the visible light absorption of photocatalysts. This has been widely reported in the field of solar cells, the production of hydrogen and the degradation of organic pollutants [14–16]. Recently, natural metal-free dyes derived from flowers, leaves, and fruits have become viable alternatives to expensive or toxic organic sensitizers because they are low-cost, easy to obtain, abundant in raw materials, and have no threat to the environment [17,18]. Many colored natural products, such as chlorophylls, carotenoids, anthocyanins, flavonoids, etc., have been used as sensitizers for TiO_2 system [19–21]. Among the large variety of natural pigments, curcumin, a natural ingredient in commercial turmeric powder, is an orange-yellow pigment, which has been widely used in physics, chemistry, biology, and medicine due to its non-toxic, biocompatible, naturally occurring characteristics [22]. In the structure of curcumin, there are two α, β unsaturated carbonyl groups at the center, which connected two phenolic groups. The β-diketone group is one of the most prominent functional groups and has an intense driving force for chelation with a metal ion. The metal complexes formed tend to be more stable than curcumin itself, which is easily degraded [23]. Moreover, curcumin has the strong absorption of a long wavelength in the visible range from 420 to 580 nm, which makes it an ideal dye sensitizer for environmental photochemical transformations in the visible light environment. For examples, Ganesh et al. [24] reported that curcumin is an effective dye in dye-sensitized solar cells (DSSC), in which the photocurrent density is 1.66 mA/cm^2. Lim et al. [25] reported the curcumin-sensitized TiO_2 composite showed significant activity in degrading organic pollutions and confirmed that the photochemical and photoelectrochemical activities of curcumin/TiO_2 are consistently higher than that of RuL_3/TiO_2 over a wide pH range. Recently, curcumin is coupled with wide band gap metal oxides, such as $Bi_{0.5}Na_{0.5}TiO_3$ and $MgO{\cdot}Al_2O_3{\cdot}ZnO$, to obtain visible light catalysts for the dye degradation [26,27]. However, it should be noted that curcumin along with other dyes attached to the TiO_2 or other oxides by simple adsorption of dyes can only be considered as a sensitizer, not a photocatalyst. The limited adsorption capacity of dyes and weak binding between dye molecules and catalysts are not conducive to rapidly transferring electrons from the dye molecules to the catalysts. Therefore, it is very meaningful to find a more suitable sensitization method to improve the photocatalytic efficiency.

In our previous works, TiO_2 nanoparticles with visible photocatalytic activity have been successfully synthesized by using anthocyanin dyes as a template during the synthesis [21,28]. The prepared TiO_2 exhibits much higher activity under visible light irradiation than under UV light. In this way, it is worthwhile to design and prepare a SiO_2/TiO_2 nanocomposite with visible photocatalytic activity by using a curcumin pigment. To the best of our knowledge, there is no report on the synthesis of SiO_2/TiO_2 nanomaterials by natural pigments at present.

In this work, a curcumin doped SiO_2/TiO_2 nanocomposite was prepared by combining supercritical drying with solvothermal-assisted crystallization, in which the curcumin pigment is directly incorporated into the structure of SiO_2/TiO_2 during the synthesis instead of external adsorption after the formation of the SiO_2/TiO_2 composites. The effects of curcumin content on microstructure,

optical, and surface electronic state of the SiO_2/TiO_2 nanocomposites were observed. The photocatalytic performance was presented by reducing Cr (VI) under visible light illumination.

2. Results and Discussion

2.1. Structure and Morphology

The XRD pattern of SiO_2/TiO_2 nanocomposites and CT (12) sample are showed in Figure 1 and Figure S1. The strong diffraction peaks at 25.3°, 37.8°, 48.0°, 55.0°, and 62.8° correspond to (101), (004), (200) (211), and (116) crystal planes of anatase TiO_2, respectively, revealing the higher crystallinity of TiO_2. For CTS (X) samples, the crystallinity of TiO_2 tended to slightly decrease with the increase of doped curcumin amount. The SiO_2 did not appear in the XRD patterns, indicating that SiO_2 existed as an amorphous phase in the nanocomposites. The average crystalline size of TS, CTS (3), CTS (6), CTS (9), CTS (12), CTS (15), and CT (12) was calculated using the Scherrer equation and the value were 9.8, 8.2, 7.5, 6.8, 6.5, 5.8, and 11.5 nm, respectively, as shown in Table 1. Obviously, the crystalline size of SiO_2/TiO_2 nanocomposites became smaller with the increase of curcumin concentration from 3 to 15%. This may be due to the formation of complexes between curcumin and the Ti atom, which effectively suppress the agglomeration and growth of TiO_2 particles, like a supramolecular template. In addition, the crystalline size of the CT (12) sample without SiO_2 was significantly greater than that of CTS (12), which indicated that SiO_2 was also responsible to suppress the aggregation and growth of the TiO_2 particles. Similar results have been reported by Hou [9] and Meng [11] et al. The textural properties and band gap of these samples in Table 1 will be presented later.

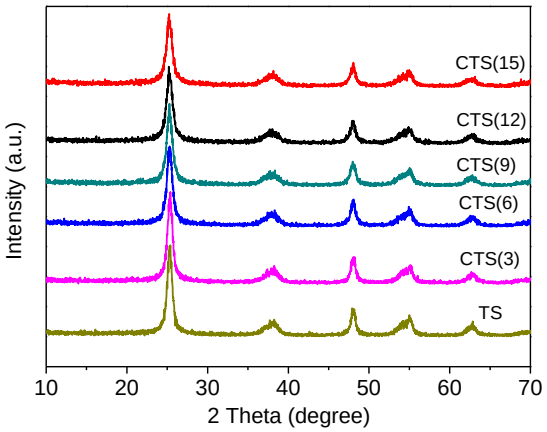

Figure 1. XRD patterns of the SiO_2/TiO_2 nanocomposites.

Table 1. Summaries of crystalline sizes, textural properties, and band gap of the samples.

Samples	Crystalline Sizes (nm)	S_{BET} (m^2g^{-1})	Pore Volume (cm^3g^{-1})	Pore Size (nm)	Eg (eV)
TS	9.8	268	0.95	18.6	3.04
CTS (3)	8.2	263	0.87	17.2	2.45
CTS (6)	7.5	270	0.77	17.2	2.37
CTS (9)	6.8	275	0.77	15.0	2.19
CTS (12)	6.5	287	0.82	15.5	2.10
CTS (15)	5.8	285	0.70	15.0	2.19
CT (12)	11.5	134	0.46	15.8	2.78

Figure 2 showed the SEM images of typical SiO_2/TiO_2 nanocomposites. It can be seen that both TS and CTS (12) nanocomposites were composed of irregular particles and displayed a similar particle accumulation pore network structure.

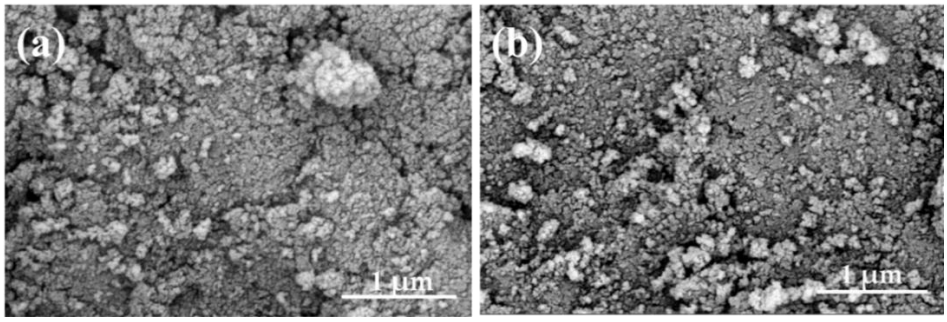

Figure 2. The SEM images of (**a**) TS and (**b**) CTS (12) samples.

Figure 3 shows the TEM images of SiO_2/TiO_2 nanocomposites with different curcumin weight ratios. It is interesting to find that the TS composite without curcumin doping actually exhibited a denser network structure than CTS (X). The dispersion of SiO_2/TiO_2 nanoparticles was obviously improved with the increase of curcumin, and highly dispersed nanoparticles were obtained when the weight ratios of curcumin were more than 6%. It is reasonable that the chelation of curcumin with Ti metal will suppress the agglomeration and growth of TiO_2 particles to a certain extent, which may be beneficial to increase the specific surface areas of the composite. Figure 3e shows the HRTEM images of CTS (12) samples, which indicate the TiO_2 particle from the CTS (12) sample was an anatase structure and its diameter was about 6 nm. This is consistent with the result by the XRD measurement. Moreover, the selected area electron diffraction (SAED) pattern in the inset of Figure 3e revealed that TiO_2 had high crystallinity. The energy dispersive X-ray spectroscopy (EDS) spectra in Figure 3f indicate that the Ti, Si, and O element existed in the SiO_2/TiO_2 nanocomposites. Moreover, carbon element appeared in samples, which confirms that curcumin was successfully doped into the SiO_2/TiO_2 nanocomposites.

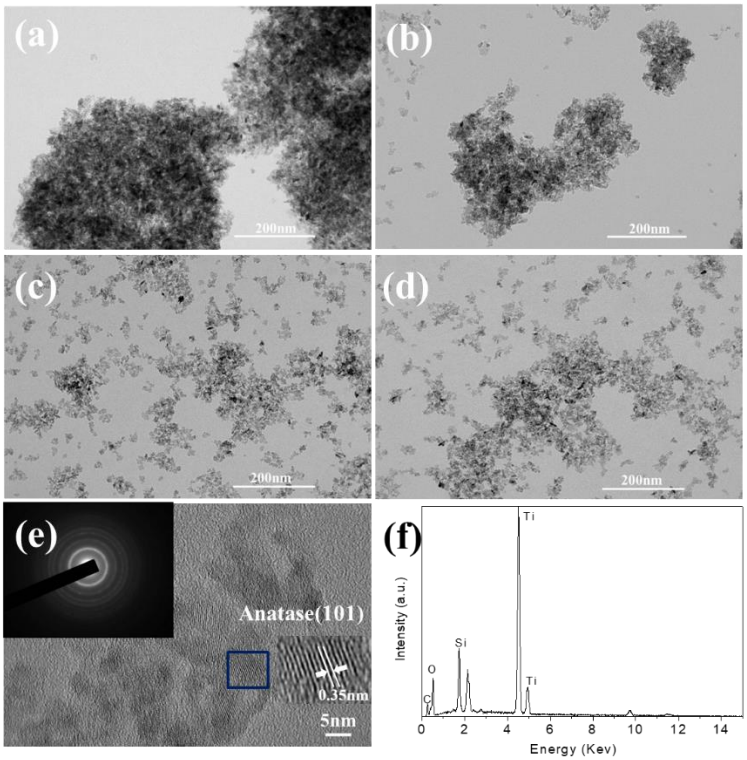

Figure 3. The TEM images of (**a**) TS, (**b**) CTS (6), (**c**) CTS (9), (**d**) CTS (12), (**e**) HRTEM image and selected area electron diffraction (SAED) of CTS (12), and (**f**) EDS of CTS (12).

The N_2 adsorption/desorption isotherms and pore size distribution curves of the SiO_2/TiO_2 nanocomposites and CT (12) sample are shown in Figure 4 and Figure S2. It is found that these samples exhibited typical type-IV isotherms having an obvious hysteresis loop at the 0.6–1.0 P/P_0 range, which demonstrated that numerous mesopores exist in the bulk phase of the SiO_2/TiO_2 nanocomposites. The pore size distribution curves in Figure 4b revealed that the pore size of the SiO_2/TiO_2 nanocomposites had a decreasing trend with the increase of the curcumin doping amount, which could be due to excessive curcumin and its decomposition residues blocking the pores. The specific surface areas, pore volumes, and pore sizes of SiO_2/TiO_2 nanocomposites were listed in Table 1. It could be found that specific surface areas of SiO_2/TiO_2 nanocomposites occur a slight increase when the weight ratios of curcumin change from 0 to 15%. By contrast, the CT (12) sample shows a lower specific BET surface area of 134 m^2g^{-1} than CTS (12) (287 m^2g^{-1}). Many reports [29,30] suggest that the addition of silica is able to improve the specific surface area of TiO_2. This would provide more surface sites for the adsorption of reactants molecules and lead to more active sites, which would contribute to the improvement of photocatalytic activity [31]. In addition, the pore size of the SiO_2/TiO_2 nanocomposites and CT (12) sample were between 15.0 and 18.6 nm in the mesoporous region.

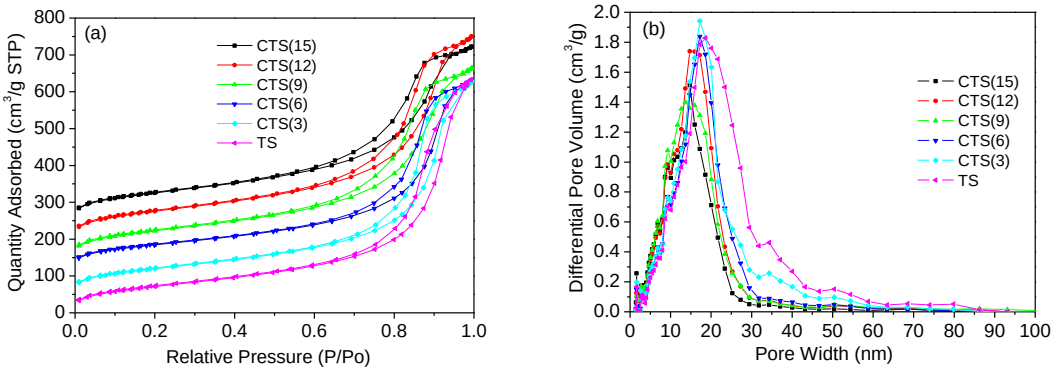

Figure 4. (**a**) N_2 adsorption/desorption curves and (**b**) pore width distribution curves of samples.

2.2. FT-IR and XPS Analyses

Figure 5 presents FTIR spectra of curcumin and SiO_2/TiO_2 nanocomposites between 500 and 4000 cm^{-1}. The IR spectrum in Figure 5a shows a characteristic band of curcumin at 3520 cm^{-1} assigned to the phenolic O–H stretching vibration. Moreover, the band at 1633 cm^{-1} can be due to the stretching vibration of benzene ring of curcumin, a band at 1510 cm^{-1} to C=O and C=C vibration, a band at 1283 cm^{-1} to the aromatic C–O stretching vibration, the band at 1000–1300 cm^{-1} to C–O–C stretching vibration [27]. The FT-IR spectrum of CTS (9) was very similar to that of pure SiO_2/TiO_2, indicating that the main structure of CTS (9) was almost identical to that of pure SiO_2/TiO_2. The bands at 830 and 1096 cm^{-1} are related to the Si–O–Si symmetric and asymmetric stretching vibration, respectively. The typical Ti–O–Ti stretching vibration due to the anatase phase is located in the region of 500–590 cm^{-1}. Moreover, the very weak band around 952 cm^{-1} is associated with the Ti–O–Si linkage, which indirectly indicates the interaction between TiO_2 and SiO_2 on the molecular scale [9]. The two broad peaks at 3420 and 1635 cm^{-1} can be attributed to the adsorption of water and hydroxyl on the surface. However, no characteristic peak of curcumin was found in CTS (9). In the case of CTS (X) samples, the FT-IR spectra were not distinctively different from each other, as shown in Figure 5b, which indicates that curcumin in the CTS (X) nanocomposites may be decomposed during the heating under nitrogen atmosphere.

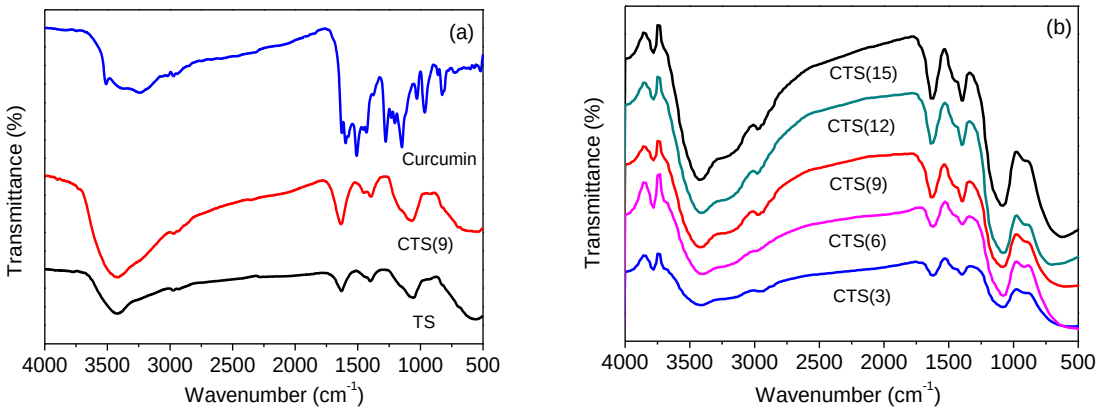

Figure 5. The FTIR spectra of (**a**) curcumin, CTS (9) and TS samples, (**b**) CTS (3), CTS (6), CTS (9), CTS (12) and CTS (15) samples.

Figure 6 shows the XPS spectra of the CTS (12) nanocomposite. The full survey spectrum in Figure 6a expounds that the nanocomposites contain the Si, Ti, O, and C element. Figure 6b shows the XPS spectrum of Ti2p, in which two peaks at 464.2 and 458.4eV were ascribed to Ti 2p1/2 and Ti 2p3/2, respectively. These values are in good agreement with Ti^{4+} in pure anatase TiO_2 [13]. Figure 6c shows the XPS spectrum of O1s, where three peaks at 529.8 eV, 531.0 eV, and 532.3 eV were assigned to Ti–O, Si–O, and O–H groups, respectively [9]. The C1s spectrum in Figure 6d can be fitted by three curves appearing at 284.8, 286.4, and 288.7 eV due to C–C (C–H), C=O, and Ti–O–C, respectively [32–34], manifesting the existence of decomposition residues from curcumin on the surface of SiO_2/TiO_2. Moreover, the atomic mass fractions in the CTS (12) and TS samples can be obtained from the curve fitting results of XPS spectra, as shown in Table 2. It is found that the mass fractions of the C atom are 23.3% and 16.1% for CTS (12) and TS, respectively, which further verifies the successful doping of curcumin into SiO_2/TiO_2.

Table 2. The atomic mass fractions obtained from the XPS analysis.

Samples	Ti2p (%)	Si2p (%)	O1s (%)	C1s (%)
TS	15.8	11.0	57.1	16.1
CTS (12)	19.6	15.2	41.9	23.3

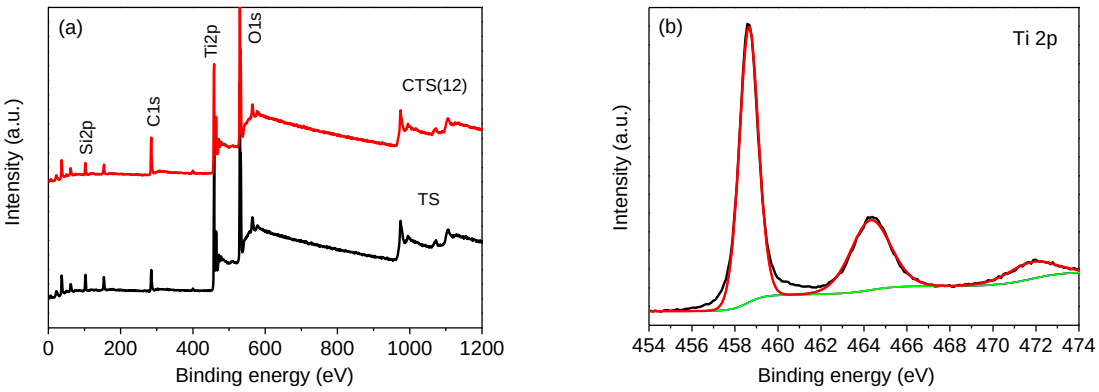

Figure 6. *Cont.*

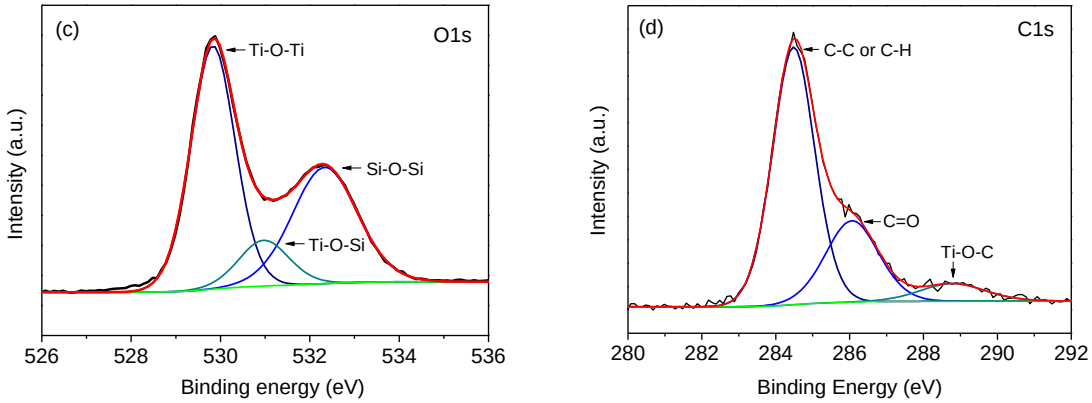

Figure 6. (**a**) XPS survey spectra of TS and CTS (12) and XPS survey spectra of CTS (12), (**b**) Ti 2p, (**c**) O 1s, and (**d**) C 1s.

2.3. UV-Vis DRS Analyses

Figure 7a presents the UV-Vis diffraction reflectance spectra of curcumin, TS, and CTS (X). Obviously, TS do not show significant absorption in the visible region from 400 to 750 nm, while the curcumin revealed significant absorption at the same region. After doping the curcumin, the absorption of CTS (X) samples in the visible range was significantly improved with the increase of curcumin content, and CTS (12) achieved maximum absorption strength. While curcumin content was 15%, the absorption of CTS (15) had a slight decline. The bandgap energies of the TS and CTS (X) samples were obtained from Tauc plots in Figure 7b. It could be found from Table 1 that the bandgap energies ranged from 3.04 eV of TS to 2.10 eV of CTS (12), indicating that the dope of curcumin could effectively narrow the bandgap energy of SiO_2/TiO_2 nanocomposites. The enhanced visible light absorption and the narrowed bandgap of CTS (X) contributed to generate photoelectron–hole pairs, further leading to the improvement of photocatalytic activity. In addition, the CT (12) sample also shows significant visible-light absorption, as shown in Figure S3, and its band gap energy was 2.78 eV, which was higher than that of CTS (12), suggesting that SiO_2 helped to decrease the bandgap energy of SiO_2/TiO_2 nanocomposites.

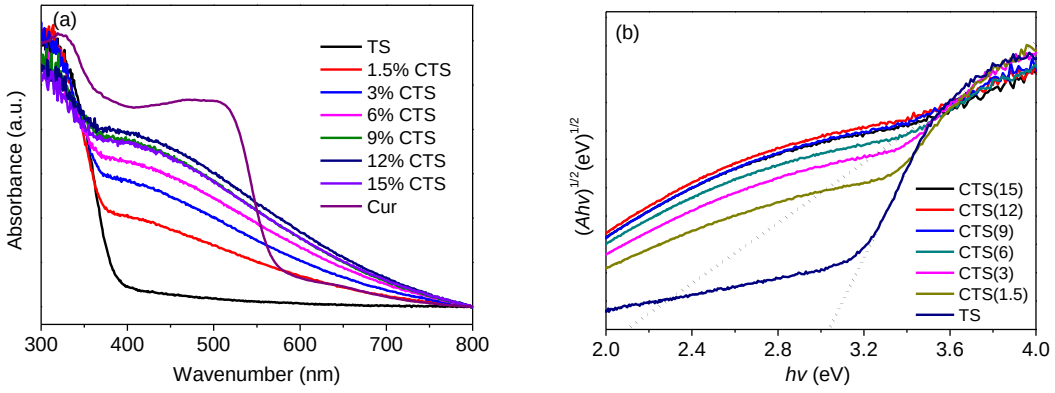

Figure 7. (**a**) UV-Vis diffuse reflectance spectra of samples and (**b**) Tauc plots for samples.

2.4. Photocatalytic Tests

2.4.1. Effect of Curcumin Doping Amount on the Photocatalytic Reduction of Cr (VI)

Figure 8 revealed the activities of the prepared samples for the photocatalytic reduction of Cr (VI) under visible light illumination. It is obvious that TS had no apparent photocatalytic activity for the reduction of Cr (VI) under visible light illumination in 2.5 h, while curcumin-doped CTS (X) samples showed an enhanced photocatalytic reduction performance. With the increase of curcumin

dosage, the photoreduction yields of Cr (VI) first increased and then decreased. The CTS (12) sample showed the best photocatalytic activity with the photocatalytic yield reaching 100% within 2.5 h. This result implies that the improved photocatalytic activities resulted from the dope of curcumin, and the introduction of a suitable amount of curcumin was beneficial to improve photocatalytic performance of SiO_2/TiO_2 composites. In fact, owing to the much stronger absorption in the visible range of CTS (X) nanocomposites than that of the TS sample, it was reasonable that curcumin-doped CTS (X) samples showed much higher photocatalytic activity than the TS sample under visible-light irradiation. Furthermore, the carbonaceous species loaded on materials were responsible for the improved photocatalytic activity. Many investigations [31,35,36] show that carbonaceous species on TiO_2 are capable of promoting direct transfer and separation of the electron. However, the CTS (15) sample with the highest doping curcumin exhibited decreased photocatalytic reduction properties, probably owing to the fact that the addition of excessive curcumin would block the pores or destroy the structural integrity of SiO_2/TiO_2, thus, may produce more recombination centers for photogenerated electron–hole pairs [16,37]. In addition, it can be found that curcumin-doped TiO_2 samples showed a 69.1% photocatalytic reduction yield under a visible-light illumination. However, in spite of the same curcumin doping amount as CTS (12), the photocatalytic reduction yield of CT (12) was still lower than that of CTS (12). The result indicates that the synergy between SiO_2 and TiO_2 in the CTS (12) nanocomposites also contributed to the improvement of photocatalytic activity.

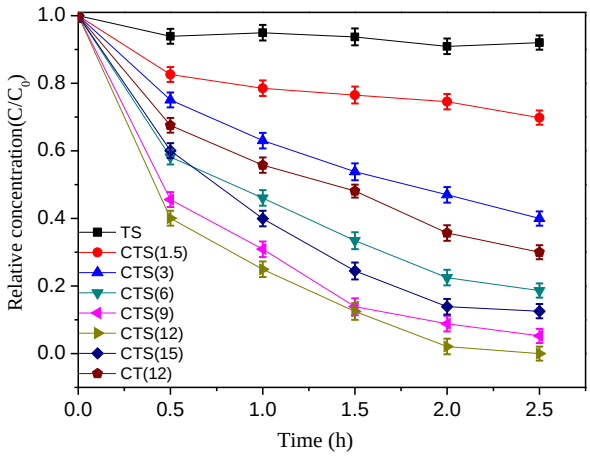

Figure 8. Photocatalytic reduction yields of Cr (VI) over different samples under visible light with 0.6 mL/L formic acid.

2.4.2. Effect of Initial Concentration on the Photocatalytic Reduction of Cr(VI)

The CTS (12) sample was used to evaluate the influence of the initial concentration on photocatalytic Cr(VI) reduction by changing initial concentration of Cr(VI) from 10 to 50 ppm with 0.6 mL/L formic acid. Figure 9 shows that the yields of photocatalytic Cr(VI) reduction decreased from 100% to 45% with increasing the initial Cr(VI) concentration after 2.5 hours. As a reason, with the increase of initial Cr(VI) concentration, more Cr(VI) ions are adsorbed on the surface of the photocatalyst. This not only prevents the absorption of light by the catalyst, but also covers the active site on the surface of the photocatalyst, thus inhibiting further photocatalytic Cr (VI) reduction [38,39].

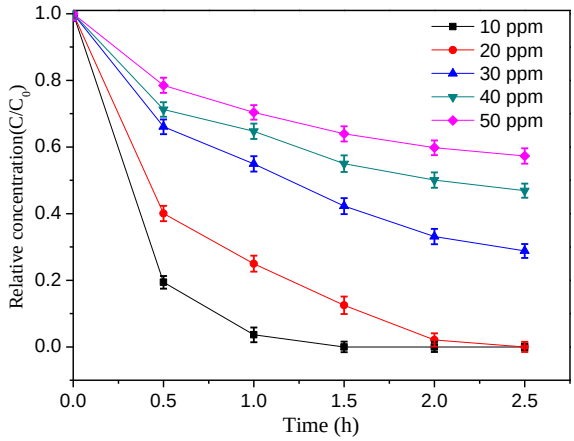

Figure 9. The photocatalytic reduction yields of Cr (VI) for different initial Cr (VI) concentration with 0.6 mL/L formic acid.

2.4.3. Effect of pH on the Photocatalytic Reduction of Cr(VI)

The pH value of the solution is one of the main factors affecting the photocatalytic reduction of Cr (VI), and the types of Cr (VI) and surface charges of the catalyst are different in different pH solutions. The adsorption of Cr (VI) over CTS (12) sample under different pH value was shown in Table 3. As was observed, the adsorption ability for Cr (VI) decreased when the pH value increased. Actually, the surface of CTS (12) carries more positive charges in acidic solution and has a strong affinity toward $HCr_2O_7^-$ anion that is the dominant species at pH 2–6. When the pH value increased, the positive charges would be less on the surface of CTS (12), which is not conducive to the attraction of $HCr_2O_7^-$ or CrO_4^{2-} with negative charges. This would lead to a lower adsorption capacity for Cr (VI), especially in the alkaline medium.

Table 3. The adsorption yields of Cr (VI) after dark reaction for 6 h.

pH	2	4	5	6	8
Adsorption Yield after dark reaction (%)	45.3	31.9	9.6	6.7	5.4

Figure 10 presents the effect of pH on photocatalytic reduction of Cr (VI) when the pH value is 2, 4, 5, 6, and 8, in which the initial Cr (VI) concentration remained the same at 20 ppm. It can be seen that the photocatalytic reduction yields were decreased with increasing the pH value of the solution. The reduction yield of Cr (VI) by CTS (12) was 100% when pH was 2, while it was only 5.0% when pH was 8. As is well known, the reduction of Cr (VI) mainly involves the following reactions:

$$\text{pH 2-6: } HCr_2O_7^- + 7H^+ + 3e^- \rightarrow Cr^{3+} + 4H_2O \quad (1)$$

$$\text{pH 7-14: } CrO_4^{2-} + 4H_2O + 3e^- \rightarrow Cr(OH)_3 + 5OH^- \quad (2)$$

So, H^+ is favorable for the Cr (VI) reduction under acidic medium, while OH^- shows the opposite effect in alkaline conditions. Therefore, the lower the pH is, the higher the photoreduction efficiency of Cr (VI) is. Similar phenomena had been observed when carbon dots-TiO_2 [35], TiO_2-graphen [40], and TiO_2-P25 [41] were used as photocatalysts. Considering that under strong acidic conditions, such as pH 2, the adsorption of Cr (VI) by CTS (12) was relatively high and was over 45%. As a result, the appropriate acidity condition for the removal of Cr (VI) was considered to be pH 4 when using CTS(X).

Additionally, compared with the results in Figure 7, the photocatalytic reduction yield under acidic conditions was much lower than that in the presence of formic acid. This means that formic acid is necessary as a sacrificial agent to capture holes and provide more electrons for Cr (VI) reduction.

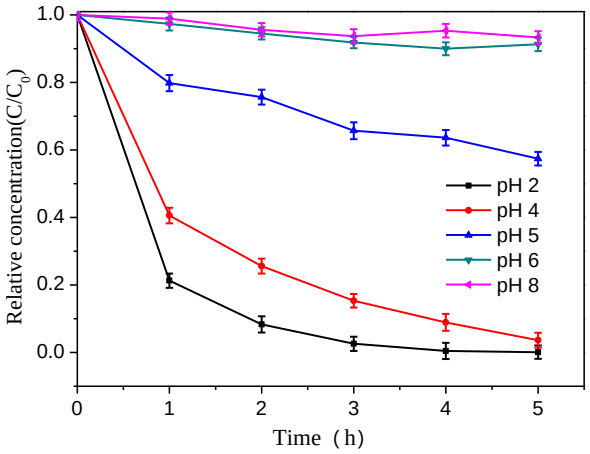

Figure 10. The yields of the photocatalytic Cr (VI) reduction under visible light in different pH solution without formic acid.

2.4.4. Recyclability of Photocatalysts

The durability of catalysts is a key criterion for practical applications, so the photocatalytic stability of CTS (12) was evaluated under visible light irradiation by a 6 h reaction during three consecutive runs. Figure 11 exhibits that the reduction yield of photocatalytic Cr (VI) could still reach 97% after three photocatalytic cycles. The result suggests that the photocatalytic activity for CTS (12) had no obvious attenuation after the cycling tests, indicating its intense antiphotocorrosion stability.

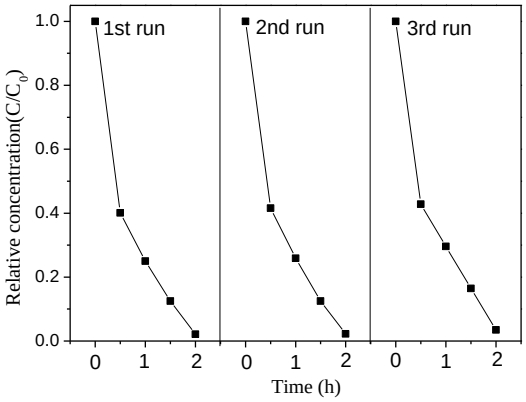

Figure 11. Recycling runs of CTS (12).

2.5. Possible Reasons for the Enchanced Visble-light Photocatalytic Activity

On the basis of the above discussion, three reasons may account for the significant photocatalytic activity of the CTS (12) under visible irradiation. First, the dope of curcumin was responsible for the far more intense adsorption of visible light. When carbonaceous species from curcumin were introduced, the band gap of CTS (X) would be narrowed, allowing the photocatalyst to absorb more visible light [32]. Second, it is generally accepted that [34,42] doped carbon in TiO_2 can act as an electron scavenging agent to reduce the recombination of the photogenerated electron–hole pair, and enhance the charge separation effect of photocatalysts. Thus, when CTS (X) was irradiated by visible light, more electrons can be provided to reduce Cr (VI) to Cr (III), while the holes would be consumed by oxidizing formic acid. Finally, the synergetic effects of SiO_2 and TiO_2 play an important role in

the improvement of photocatalytic performance. As described above, besides curcumin, SiO_2 also contributes to improve specific surface area and narrow the bandgap energy of CTS (12). So, it is reasonable that absorption towards visible light for CTS (12) is far more than that of CT (12). Moreover, CTS (12) with large specific surface area can not only improve the adsorption of reactants molecules, which is usually the first step of the photocatalytic reaction, but also provide more active sites to accelerate the diffusion and transition of reactants during photocatalysis [29,31,43,44], all which are beneficial to the improvement of photocatalytic performance. Therefore, the significantly enhanced visible photocatalytic activity may be due to the curcumin doping and the synergetic effects of SiO_2 and TiO_2 in SiO_2/TiO_2 nanocomposites.

3. Materials and Methods

3.1. Synthesis

The curcumin was provided by Yunnan Tonghai Yang Natural Products Co., LTD (Yuxi, China). Titanium isopropylate and tetraethyl orthosilicate was bought from Aladdin Industrial Inc. (Shanghai, China).

Curcumin doped SiO_2/TiO_2 nanocomposites were prepared by a modified process [21,28]. Different amounts of curcumin was dissolved in 50 mL of ethanol, 5 mL tetraethyl orthosilicate and 15 mL titanium isopropylate were added in turn under stirring, then the mixture of 0.1 mL nitric acid and 4 mL deionized water was added to the above solution drop by drop and continued to stir for 30 min. The obtained mixture was aged into a gel at room temperature for 24 h. The gel was transferred into an autoclave and dehydrated at 245 °C for 2 h under nitrogen atmosphere. Before being cooled down to room temperature, the sample was rinsed again with nitrogen for another 15 min. The final products were collected for use without further processing. A series of SiO_2/TiO_2 samples (denoted as CTS(X), X is the amount of curcumin, and X = 3 wt %, 6 wt %, 9 wt %, 12 wt %, and 15 wt %, respectively) were prepared by changing the content of curcumin in the precursor. For comparison, the pure SiO_2/TiO_2 nanocomposite without adding curcumin and TiO_2 sample with 12 wt % curcumin was prepared according to the same procedure, which was denoted as CTS and CT (12), respectively.

3.2. Characterizations

X-ray diffraction (XRD) data were obtained on a Rigaku TTRAX III spectrometer with Cu Kα radiation (Rigaku Co., Tokyo, Japan) with a scanning angle between 10 and 80° at a rate of 10°/min. Scanning electron microscopy (SEM) characterizations were carried out by a FEI Quanta 200 ESEM (FEI, Hillsboro, OR, USA) with an accelerating voltage of 10 kV. Transmission electron microscopy (TEM) images were analyzed by a JEM-2100 (Japan Electron Optics Laboratory CO., Ltd., Tokyo, Japan) operated at 200 kV. The specific surface areas were determined by a Micromeritics Tristar II Surface Area and Porosity Analyzer (Micromeritics, Norcross, GA, USA). Fourier transform infrared (FTIR) spectra were obtained on a Thermo Nicolet 8700 instrument (Thermo Fisher Scientific, Waltham, MA, USA). The light absorption spectra of the samples were recorded using a Shimadzu UV2600 spectrophotometer (Shimadzu Corp., Kyoto, Japan) over the 200–800 nm range. The X-ray photoelectron spectroscopy (XPS) experiment was performed using a PHI5500ESCA (Thermo Fisher Scientific Inc., Waltham, MA, USA) spectrophotometer with the 200 W Mg Kα source.

3.3. Photocatalytic Activity

Photocatalytic reactions were performed in a quartz photoreactor. The photocatalyst of 25 mg was added to a 50 mL 10–50 ppm Cr (VI) aqueous solution with 0.6 mL/L formic acid. The solution pH value was adjusted to 2.0–8.0 with 0.2 M of HCl or 0.2 M of NaOH. The suspensions were transferred in a quartz photoreactor and magnetically stirred kept for 6 h under dark conditions to achieve adsorption–desorption equilibrium. The photocatalytic process was initiated by exposing the suspensions under visible light using the 350 W Xe lamp with a 420 nm cut-off filter. During light

exposure, cold water was circulated around the photoreactor to maintain room temperature. At scheduled time intervals, the samples were collected from the reactor during illumination and then filtered through a 0.45 mm PTFE syringe filter to remove the powder samples. The concentrations of Cr (VI) were measured using a UV-Vis spectrophotometer at 540 nm.

4. Conclusions

In summary, the curcumin-doped SiO_2/TiO_2 nanocomposites were prepared by directly incorporating it into the structure of SiO_2/TiO_2 during the synthesis using an inexpensive and readily available natural pigment (curcumin) as the doping agent, rather than conventional photosensitization by adsorbing. Curcumin could reduce the crystal sizes and slightly increase the specific surface area, by contrast, the visible absorbance of SiO_2/TiO_2 could be enhanced remarkably, which was related with the content of doped curcumin. The appropriate curcumin in SiO_2/TiO_2 was conducive to enhance the visible photocatalytic activity. In particular, CTS (12) nanocomposites with the content of curcumin of 12 wt % exhibited the best visible-light photocatalytic activity for the reduction of Cr (VI) in the solution. This can be ascribed to the curcumin doping and the synergetic effects of SiO_2 and TiO_2 in SiO_2/TiO_2 nanocomposites. CTS (12) also showed excellent stability and did not lose significant activity after being reused 3 times. Furthermore, this approach is simpler and provides new thought for the design of the visible light catalysts with high efficiency for environmental applications, specifically for the treatment of polluted water applications.

Supplementary Materials: The following are available online at http://www.mdpi.com/2073-4344/10/8/942/s1, Figure S1: XRD pattern of the CT (12) sample, Figure S2: (a) N_2 adsorption/desorption isotherm and (b) pore width distribution curve of CT (12) sample, Figure S3: (a) UV-Vis diffuse reflectance spectrum and (b) the bandgap energy for CT (12) sample.

Author Contributions: The design of the study, Z.Y. and J.W.; the writing of the manuscript, Z.Y.; the collection of data Z.H. and Y.L.; the analyses or interpretation of data, J.H. and Y.C.; the revision of the manuscript, M.L. and L.Z. All authors have read and agreed to the published version of the manuscript.

Funding: This research was funded by YUNNAN APPLIED BASIC RESEARCH PROJECT, grant number 2016FA002, 2018FB013 and NATIONAL NATURAL SCIENCE FOUNDATION OF CHINA, grant number 21773204.

Conflicts of Interest: The authors declare no conflict of interest.

References

1. Hoffmann, M.R.; Martin, S.T.; Choi, W.; Bahnemann, D.W. Environmental applications of semiconductor photocatalysis. *Chem. Rev.* **1995**, *95*, 69–96. [CrossRef]
2. Schneider, J.; Matsuoka, M.; Takeuchi, M.; Zhang, J.; Horiuchi, Y.; Anpo, M.; Bahnemann, D.W. Understanding TiO_2 photocatalysis: Mechanisms and materials. *Chem. Rev.* **2014**, *114*, 9919–9986. [CrossRef] [PubMed]
3. Zhang, J.; Zhou, P.; Liu, J.; Yu, J. New understanding of the difference of photocatalytic activity among anatase, rutile and brookite TiO_2. *Phys.Chem. Chem. Phys.* **2014**, *16*, 20382–20386. [CrossRef] [PubMed]
4. Humayun, M.; Raziq, F.; Khan, A.; Luo, W. Modification strategies of TiO_2 for potential applications in photocatalysis: A critical review. *Green Chem. Lett. Rev.* **2018**, *11*, 86–102. [CrossRef]
5. Anderson, C.; Bard, A.J. An improved photocatalyst of TiO_2/SiO_2 prepared by a Sol-Gel synthesis. *J. Phys. Chem.* **1995**, *99*, 9882–9885. [CrossRef]
6. Kang, C.; Jing, L.; Guo, T.; Cui, H.; Zhou, J.; Fu, H. Mesoporous SiO_2-modified nanocrystalline TiO_2 with high anatase thermal stability and large surface area as efficient photocatalyst. *J. Phys. Chem. C* **2009**, *113*, 1006–1013. [CrossRef]
7. Mahesh, K.P.O.; Kuo, D.H.; Huang, B.R.; Ujihara, M.; Imae, T. Chemically modified polyurethane-SiO_2/TiO_2 hybrid composite film and its reusability for photocatalytic degradation of Acid Black 1 (AB 1) under UV light. *Appl. Catal. A Gen.* **2014**, *475*, 235–241. [CrossRef]
8. Li, Z.J.; Hou, B.; Xu, Y.; Wu, D.; Sun, Y.H. Hydrothermal synthesis, characterization, and photocatalytic performance of silica modified titanium dioxide nanoparticles. *J. Colloids Interface Sci.* **2005**, *288*, 149–154. [CrossRef]

9. Hou, Y.D.; Wang, X.C.; Wu, L.; Chen, X.F.; Ding, Z.X.; Wang, X.X.; Fu, X.Z. N-Doped SiO_2/TiO_2 mesoporous nanoparticles with enhanced photocatalytic activity under visible-light irradiation. *Chemosphere* **2008**, *72*, 414–421. [CrossRef]
10. Mahyar, A.; Behnajady, M.A.; Modirshahla, N. Characterization and photocatalytic activity of SiO_2–TiO_2 mixed oxide nanoparticles prepared by sol–gel method. *Indian. J. Chem. A* **2010**, *49*, 1593–1600.
11. Meng, X.; Qian, Z.; Wang, H.; Gao, X.; Zhang, S.; Yang, M. Sol–gel immobilization of SiO_2/TiO_2 on hydrophobic clay and its removal of methyl orange from water. *J. Sol-Gel. Sci. Tech.* **2008**, *46*, 195–200. [CrossRef]
12. Ghanbari1, S.; Givianrad, M.H.; Azar, P.A. Synthesis of N-F-codoped TiO_2/SiO_2 nanocomposites as a visible and sunlight response photocatalyst for simultaneous degradation of organic water pollutants and reduction of Cr (VI). *J. Sol-Gel Sci. Techn.* **2019**, *89*, 562–570. [CrossRef]
13. Liu, J.; Liu, J.; Shi, F.; Hu, S.; Jiang, S.; Liu, S.; Liu, D.; Tian, X. F/W co-doped SiO_2-TiO_2 composite aerogels with improved visible light-driven photocatalytic activity. *J. Solid State Chem.* **2019**, *275*, 8–15. [CrossRef]
14. Liang, M.; Chen, J. Arylamine organic dyes for dyesensitized solar cells. Chem. *Soc. Rev.* **2013**, *42*, 3453–3488. [CrossRef] [PubMed]
15. Venkateswararao, A.; JustinThomas, K.R.; Lee, C.P.; Li, C.T.; Ho, K.C. Organic dyes containing carbazole as donor and π-Linker: Optical, electrochemical, and photovoltaic properties. *ACS Appl. Mater. Interfaces.* **2014**, *6*, 2528–2539. [CrossRef]
16. Wang, Z.; Lang, X. Visible light photocatalysis of dye-sensitized TiO_2: The selective aerobic oxidation of amines to imines. *Appl. Catal. B Environ.* **2018**, *224*, 404–409. [CrossRef]
17. Zhang, S.; Yang, X.; Numata, Y.; Han, L. Highly efficient dye-sensitized solar cells: Progress and future challenges. *Energy Environ. Sci.* **2013**, *6*, 1443–1464. [CrossRef]
18. Shalini, S.; Balasundaraprabhu, R.; Kumar, T.S.; Prabavathy, N.; Senthilarasu, S.; Prasanna, S. Status and outlook of sensitizers/dyes used in dye sensitized solar cells (DSSC): A review. *Int. J. Energy Res.* **2016**, *40*, 1303–1320. [CrossRef]
19. Wongcharee, K.; Meeyoo, V.; Chavadej, S. Dye-sensitized solar cell using natural dyes extracted from rosella and blue pea flowers. *Sol. Energ. Mat. Sol. C.* **2007**, *91*, 566–571. [CrossRef]
20. Maiaugree, W.; Lowpa, S.; Towannang, M.; Rutphonsan, P.; Tangtrakarn, A.; Pimanpang, S.; Maiaugree, P.; Ratchapolthavisin, N.; Sang-Aroon, W.; Jarernboon, W.; et al. A dye sensitized solar cell using natural counter electrode and natural dye derived from mangosteen peel waste. *Sci. Rep.* **2015**, *5*, 15230. [CrossRef]
21. Yang, H.; Jiang, L.; Li, Y.; Li, G.; Yang, Y.; He, J.; Wang, J.; Yan, Z. Highly efficient red cabbage anthocyanin inserted TiO_2 aerogel nanocomposites for photocatalytic reduction of Cr(VI) under visible light. *Nanomaterials* **2018**, *8*, 937. [CrossRef] [PubMed]
22. Wanninger, S.; Lorenz, V.; Subhan, A.; Edelmann, F.T. Metal complexes of curcumin—Synthetic strategies, structures and medicinal applications. *Chem. Soc. Rev.* **2015**, *44*, 4986–5002. [CrossRef] [PubMed]
23. Pröhl, M.; Schubert, U.S.; Weigand, W.; Gottschaldt, M. Metal complexes of curcumin and curcumin derivatives for molecular imaging and anticancer therapy. *Coordin. Chem. Rev.* **2016**, *307*, 32–41. [CrossRef]
24. Ganesh, T.; Kim, J.H.; Yoon, S.J.; Kil, B.; Maldar, N.N.; Han, J.W. Photoactive curcumin-derived dyes with surface anchoring moieties used in ZnO nanoparticle-based dye-sensitized solar cells. *Mater. Chem. Phys.* **2010**, *123*, 62–66. [CrossRef]
25. Lim, J.; Bokare, A.D.; Choi, W. Visible light sensitization of TiO_2 nanoparticles by a dietary pigment, curcumin, for environmental photochemical transformations. *RSC Adv.* **2017**, *7*, 32488–32495. [CrossRef]
26. Kushwaha, H.S.; Vaish, R. Enhanced visible light photocatalytic activity of curcumin-sensitized perovskite $Bi_{0.5}Na_{0.5}TiO_3$ for rhodamine 6G degradation. *Int. J. Appl. Ceram. Technol.* **2016**, *13*, 333–339. [CrossRef]
27. Subhan, M.A.; Saha, P.C.; Uddin, N.; Sarker, P. Synthesis, structure, spectroscopy and photocatalytic studies of nano multimetal oxide $MgO{\cdot}Al_2O_3{\cdot}ZnO$ and $MgO{\cdot}Al_2O_3{\cdot}ZnO$ curcumin composite. *Int. J. Nanosci. Nanotechnol.* **2017**, *13*, 69–82.
28. Yan, Z.; Gong, W.; Chen, Y.; Duan, D.; Li, J.; Wang, W.; Wang, J. Visible-light degradation of dyes and phenols over mesoporous titania prepared by using anthocyanin from red radish as template. *Inter. J. Photoenergy* **2014**, *2014*, 1–10. [CrossRef]
29. Dorian, A.H.H.; Sorrell, C.C. Sand supported mixed-phase TiO_2 photocatalysts for water decontamination applications. *Adv. Eng. Mater.* **2014**, *16*, 248–254.

30. Kibombo, H.S.; Zhao, D.; Gonshorowski, A.; Budhi, S.; Koppang, M.D.; Koodali, R.T. Cosolvent-induced gelation and the hydrothermal enhancement of the crystallinity of titania-silica mixed oxides for the photocatalytic remediation of organic pollutants. *J. Phys. Chem. C* **2011**, *115*, 6126–6135. [CrossRef]
31. Lin, X.; Rong, F.; Ji, X.; Fu, D. Carbon-doped mesoporous TiO_2 film and its photocatalytic activity. *Micropor. Mesopor. Mater.* **2011**, *142*, 276–281. [CrossRef]
32. Shao, J.; Sheng, W.; Wang, M.; Li, S.; Chen, J.; Zhang, Y.; Cao, S. In situ synthesis of carbon-doped TiO_2 single-crystal nanorods with a remarkably photocatalytic efficiency. *Appl. Catal. B Environ.* **2017**, *209*, 311–319. [CrossRef]
33. Wang, H.; Liu, H.; Wang, S.; Li, L.; Liu, X. Influence of tunable pore size on photocatalytic and photoelectrochemical performances of hierarchical porous TiO_2/C nanocomposites synthesized via dual-templating. *Appl. Catal. B Environ.* **2018**, *224*, 341–349. [CrossRef]
34. Fu, X.; Yang, H.; Sun, H.; Lu, G.; Wu, J. The multiple roles of ethylenediamine modification at TiO_2/activated carbon in determining adsorption and visible-light-driven photoreduction of aqueous Cr (VI). *J. Alloys Compd.* **2016**, *662*, 165–172. [CrossRef]
35. Li, Y.; Liu, Z.; Wu, Y.; Chen, J.; Zhao, J.; Jin, F.; Na, P. Carbon dots-TiO_2 nanosheets composites for photoreduction of Cr(VI) under sunlight illumination: Favorable role of carbon dots. *Appl. Catal. B Environ.* **2018**, *224*, 508–517. [CrossRef]
36. Janus, M.; Inagaki, M.; Tryba, B.; Toyoda, M.; Morawski, A.W. Carbon-modified TiO_2 photocatalyst by ethanol carbonisation. *Appl. Catal. B Environ.* **2006**, *63*, 272–276. [CrossRef]
37. Ren, Z.; Liu, X.; Chu, H.; Yu, H.; Xu, Y.; Zheng, W.; Lei, W.; Chen, P.; Li, J.; Li, C. Carbon quantum dots decorated $MoSe_2$ photocatalyst for Cr(VI) reduction in the UV–vis-NIR photon energy range. *J. Colloid Interface Sci.* **2017**, *488*, 190–195. [CrossRef]
38. Mohammad, N.J.; Mehdi, S.S.; Yang, J.K.; Gholami, M.; Farzadkia, M. Photocatalytic reduction of hexavalent chromium with illuminated ZnO/TiO_2 composite. *J. Ind. Eng. Chem.* **2015**, *22*, 317–322.
39. Liu, X.; Pan, L.; Zhao, Q.; Lv, T.; Zhu, G.; Chen, T.; Lu, T.; Sun, Z.; Sun, C. UV-assisted photocatalytic synthesis of ZnO–reduced graphene oxide composites with enhanced photocatalytic activity in reduction of Cr(VI). *Chem. Eng. J.* **2012**, *183*, 238–243. [CrossRef]
40. Li, Y.; Cui, W.; Liu, L.; Zong, R.; Yao, W.; Liang, Y.; Zhu, Y. Removal of Cr(VI) by 3D TiO_2-graphene hydrogel via adsorption enriched with photocatalytic reduction. *Appl. Catal. B Environ.* **2016**, *199*, 412–423. [CrossRef]
41. Belisa, A.M.; Ridha, D.; Raquel, O.C.; José, M.L.; Rui, A.R.B.; Madalena, M.D.; José Carlos, B.L.; Vítor, J.P.V. Intensification of heterogeneous TiO_2 photocatalysis using an innovative micro–meso-structured-reactor for Cr(VI) reduction under simulated solar light. *Chem. Eng. J.* **2017**, *318*, 76–88.
42. Liu, F.; Yu, J.; Tu, G.; Qu, L.; Xiao, J.; Liu, Y.; Wang, L.; Lei, J.; Zhang, J. Carbon nitride coupled Ti-SBA15 catalyst for visible-light-driven photocatalytic reduction of Cr (VI) and the synergistic oxidation of phenol. *Appl. Catal. B Environ.* **2017**, *201*, 1–11. [CrossRef]
43. Anderson, C.; Bard, A.J. Improved photocatalytic activity and characterization of mixed TiO_2/SiO_2 and TiO_2/Al2O_3 materials. *J. Phys. Chem.* **1997**, *101*, 2611–2616. [CrossRef]
44. Jafry, H.R.; Liga, M.V.; Li, Q.; Barron, A.R. Simple route to enhanced photocatalytic activity of P25 titanium dioxide nanoparticles by silica addition. *Environ. Sci. Technol.* **2011**, *45*, 1563–1568. [CrossRef] [PubMed]